

1 **Seismicity rate changes and geodetic transients in Central Apennines**

2

3 **Blaž Vičić¹, Abdelkrim Aoudia¹, Alessandra Borghi^{1,2} Seyyedmaalek Momeni¹, Alessandro**
4 **Vuan³**

5

6 ¹ The Abdus Salam International Centre for Theoretical Physics, Italy

7 ² Istituto Nazionale Geofisica e Vulcanologia, sezione di Bologna, Italy

8 ³ National Institute of Oceanography and Applied Geophysics - OGS, Italy

9

10 Blaž Vičić (bvicic@ictp.it)

11

12 **Key Points:**

- 13 • Sub-horizontal shear zone beneath the shallow normal faults of Central Apennines is
14 segmented into high and low seismicity rate strands
- 15 • Rate changes in seismicity are time-correlated with a transient deformation observed
16 before the 2016 Central Italy sequence
- 17 • Mw5+ earthquakes on the Campotosto fault highlight a connection between high rate
18 shear zone segments and locked fault patches

19

20

21 **Abstract**

22 Using template matching and GPS data, we investigate the evolution of seismicity and observable
23 deformation in Central Apennines. Seismicity appears more persistent at the base of the
24 seismogenic layer than in the shallower crust. Diffuse activity is reported on segments at depth,
25 alternating along strike with apparent quiescence on segments that experienced one or more Mw6+
26 earthquakes in 1997, 2009 and 2016. Central Apennines are likely underlain by a sizeable shear
27 zone with areas of diffuse seismicity bounding shallow normal faults where Mw6+ earthquakes
28 occurred. The deformation observed at the surface seems to follow the seismicity variations at the
29 base of seismogenic layer along the Apenninic chain. Principal and independent component
30 analysis of GPS data exhibits a transient when the 2016 foreshock sequence starts. This transient
31 propagated northward from the Campotosto fault up to the Alto Tiberina fault system and has
32 likely loaded the Mw6+ 2016 earthquake sequence.

33

34 **Plain Language Summary**

35 We use a non-standard method for the detection of microseismicity at depth augmenting the
36 available catalog. The enhanced seismicity distribution is coupled with the observable deformation
37 on a geodetic network of continuous GPS to infer a better comprehension of the earthquake
38 behaviour. The earthquake patterns in Central Apennines reveal a segmentation at depth along an
39 almost flat base of seismogenic layer with alternating low and high seismicity rate segments. The
40 deformation recorded at the surface seems to follow the seismicity variations at the base of
41 seismogenic layer along the Apenninic chain also determining a possible seismic-aseismic mode.
42 We suggest that aseismic deformation has a fundamental role in the tectonic loading and that
43 seismicity, even if heterogeneously distributed, could represent a tracer of it. This conclusion is
44 also supported by the evidence of a transient propagating from south to north during the 2016
45 Central Italy sequence.

46

47 1 Introduction

48 Historical and recent destructive earthquakes in the Central Apennines, Italy (Amato et al., 1998;
49 Chiaraluce et al., 2017; Rovida et al., 2011; Valoroso et al., 2013) occur mostly along the NW-SE
50 trending system of normal faults, where 2 to 3 mm/year of extension perpendicular to the
51 Apennines is accommodated (D'Agostino et al., 2011). The fault system is located above a
52 delaminating Adria lithosphere (Aoudia et al. 2007; Chimera et al., 2003).

53 Central Apennines were recently struck by three destructive earthquake sequences, namely
54 Umbria-Marche 1997, L'Aquila 2009 and Amatrice-Visso-Norcia 2016-2017. A number of
55 foreshocks and aftershocks was relocated using both continuous and temporary networks (Amato
56 et al., 1998; Chiaraluce et al., 2011; Improta et al., 2019; Valoroso et al., 2013; Vuan et al., 2017)
57 to depict the geometry of the system. The relocated catalogues of L'Aquila and Amatrice-Visso-
58 Norcia sequences show a sub-horizontal, east-dipping Shear Zone (SZ) at the base of the
59 seismogenic volume, between 8 and 12 km. The sub-horizontal geometry of SZ is confirmed by
60 focal solutions of foreshocks and aftershocks at the base of Campotosto and Monte Vettore faults
61 (Chiaraluce et al., 2017; Improta et al., 2019; Valoroso et al., 2013). Seismic profiles and geologic
62 cross-sections show a horizontal SZ between 8 and 11 km as a transition from sedimentary into
63 basement units (e.g. Porreca et al. 2018). This transition corresponds to the observed velocity
64 changes underneath L'Aquila and Amatrice-Visso-Norcia sequences inferred by earthquake
65 travel-time tomography (Buttinelli et al. 2018; Chiarabba et al. 2018).

66 Before the L'Aquila 2009 mainshock, a foreshock sequence started in the area adjacent to the
67 nucleation point of the Mw6.3 mainshock (Valoroso et al., 2013). Sukan et al. (2014) identified
68 three phases of foreshock migration towards the nucleation point of the April 6th 2009 mainshock,
69 with one in mid-February interpreted as a slow-slip transient. The same transient was identified
70 using GPS data by Borghi et al. (2016), who attributed it to a M6.1 slow-slip event. It was
71 suggested that the transient took place over a sub-horizontal SZ at the base of Paganica and
72 Campotosto faults involving the lateral extent of the aftershock sequence. Before the Amatrice,
73 August 24th 2016 earthquake, Vuan et al. (2017) proposed that slip along the SZ increased the
74 stress around the source area of the mainshock, contributing to the unlocking of the overlying
75 normal faults.

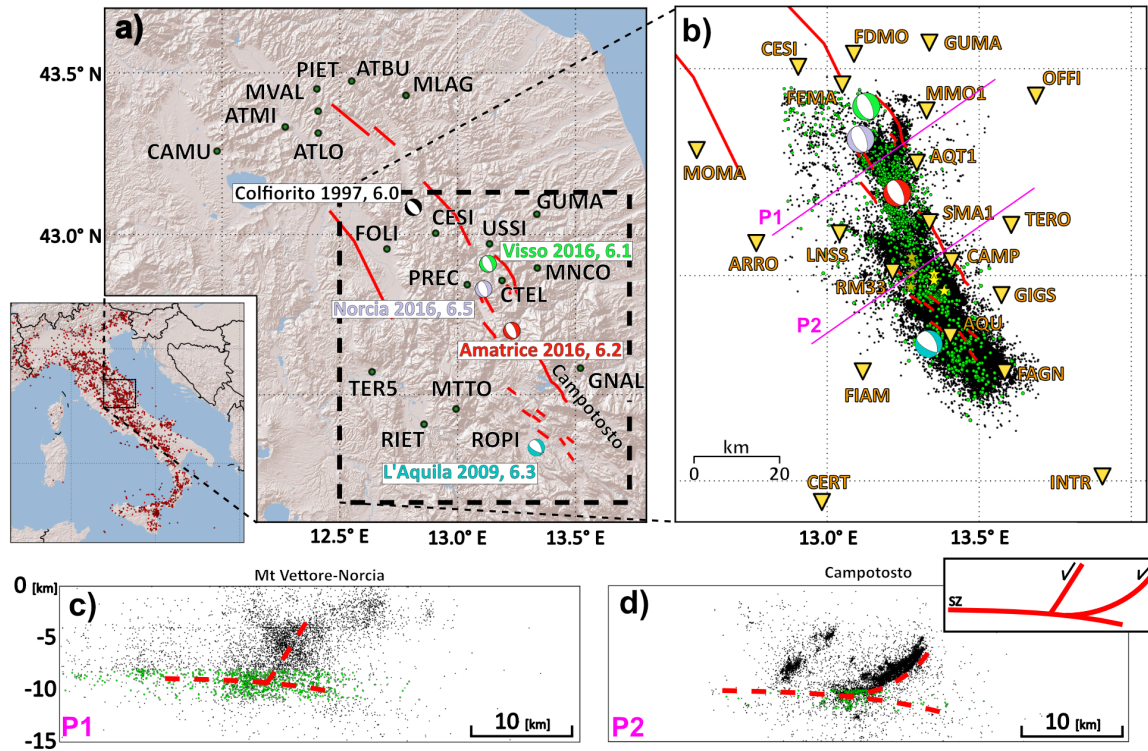


Figure 1: Studied area of Central Italy. a) Map of destructive earthquakes since 1997 in the studied area. Beach ball colours refer to the same events in figure 1a, b. Red lines represent causative faults responsible for the mainshocks. In green we plot the continuous GPS stations. b) Triangles represent seismic stations used in this study. Black dots are earthquakes of 2009 L'Aquila and 2016 Amatrice-Visso-Norcia sequences. With green we show selected template earthquakes. c) and d) are cross-sections over Amatrice-Visso-Norcia and L'Aquila epicentral areas. In d) we show an idealized profile over the area with normal faults, mature listric faults and shear-zone.

76
77
78
79
80
81
82

83 Among the mentioned faults, the geometry and seismic potential of the Campotosto fault (Fig 1a,
84 d) (hereafter Cf) for producing large earthquakes has been debatable, especially after the 2009 and
85 2016-2017 Mw5+ events (i.e. Chiaraluce et al., 2011; Cheloni et al., 2014; Cheloni et al., 2019;
86 Falcucci et al., 2018; Gualandi et al., 2014; Valoroso et al., 2013).
87 Cf is situated in the western flank of the Laga Mountains, with a northwest strike and dips towards
88 the southwest with a listric geometry, as suggested from seismic data (Chiaraluce et al., 2011).
89 Morpho-tectonic evidence confirms that Cf has different kinematics than its neighbouring
90 Paganica and Mt Vettore-Norcia faults towards southeast and northwest, respectively (Falcucci et
91 al., 2018). Cf is bounded at a depth of 10 km by SZ (Valoroso et al., 2013) and could be capable
92 of producing an M6.4-6.6 earthquake (Falcucci et al., 2018). Two historical earthquakes on Cf
93 were reported (Galadini and Galli, 2003) over the past ~8 ka, with ~1 m of minimum vertical slip.
94 We investigate both seismicity and deformation observed by the geodetic network of the Central
95 Apennines. We exploit waveform similarity over 11 years from 2008 until the beginning of 2019
96 to define the spatial and temporal evolution of detected earthquakes within the SZ and its relation
97 to the reactivated normal faults. To understand the geometry of Cf we invert the extended source
98 ruptures of eight ($4.4 \leq M \leq 5.4$) earthquakes of the 2009 and 2017 sequences (Fig 1b). We perform
99 a principal component analysis and variational Bayesian Independent Component Analysis of all
100 available continuous GPS (cGPS) stations in the broader region of Central Apennines between
101 January 1st 2015 until August 24th 2016 to detect possible geodetic transients and investigate their

102 significance together with seismicity variations. We study seismicity pattern of the SZ in the
103 broader area of Central Apennines and compare it with our results.

104 **2 Methods**

105 **2.1 Template matching**

106 We analyse the period from 2008 to the beginning of 2019 using only well relocated foreshocks
107 and aftershocks of 2009 (Valoroso et al., 2013) and 2016 (Vuan et al., 2017) mainshocks (Fig 1b).
108 These selected events nucleated beneath the computed slip distribution of the mainshocks (Walters
109 et al., 2018) within the SZ at depths between 10–12 km and 8–11 km for 2009 and 2016
110 respectively. The merged earthquake catalog (Fig S2, S3) was used in template matching (Gibbons
111 & Ringdal, 2006; Ross et al., 2019; Shelly et al., 2007) to detect collocated earthquakes and
112 transients (Vičić et al., 2019) within the SZ. Daylong waveform data of selected stations (Fig 1b)
113 are downsampled to 20 Hz and filtered between 2-8 Hz. For each event, we compute the theoretical
114 S-wave arrival time (Krischer et al., 2015) using a suitable velocity model (Herrmann et al., 2011)
115 and trim the 3 component data in 5 seconds waveforms centred on this arrival. We extract the
116 templates for the four closest stations. The signal to noise ratio of templates is evaluated by using
117 simple Kurtosis-based (Baillard et al., 2014). Templates that do not satisfy the Kurtosis test, or are
118 visual bad, are removed. Template matching detection algorithm as described in Vuan et al. (2018)
119 is applied. For positive detection we set a threshold of 12 times median absolute deviation of the
120 daily stacked cross-correlation function. We only select detected events with inter-event times > 3
121 seconds to not count same events as multiple due to the detections from different templates.
122 Selected detection inside this time window is the one with highest threshold value. The magnitude
123 of the detection is calculated as the median value of the maximum amplitude ratio for all channels
124 between the template and detected event where a 10-fold increase in amplitude corresponds to a
125 unit increase in magnitude (Peng, et al. 2009).

126 **2.2 Extended source inversion**

127 We invert near-field three-component strong motion records of 8 earthquakes ($4.4 \leq M \leq 5.4$) that
128 occurred on the Cf during 2009 and 2017 sequences to study the kinematics of the ruptured area
129 and constrain the geometry of Cf and discuss its seismogenic potential. The elliptical sub-fault
130 approximation method (Di Carli et al., 2010; Twardzik et al., 2012; Ruiz & Madariaga, 2013;
131 Momeni et al., 2019) is used to retrieve the robust features of the ruptures. For each rupture we
132 look for the best waveform-fit to the observations (Figs. Sa1 to Sa7 in Appendix-A) and infer the
133 geometry of the Cf along strike and dip. The details of our inversions are presented in Appendix-
134 A and B.

135 **2.3 GPS**

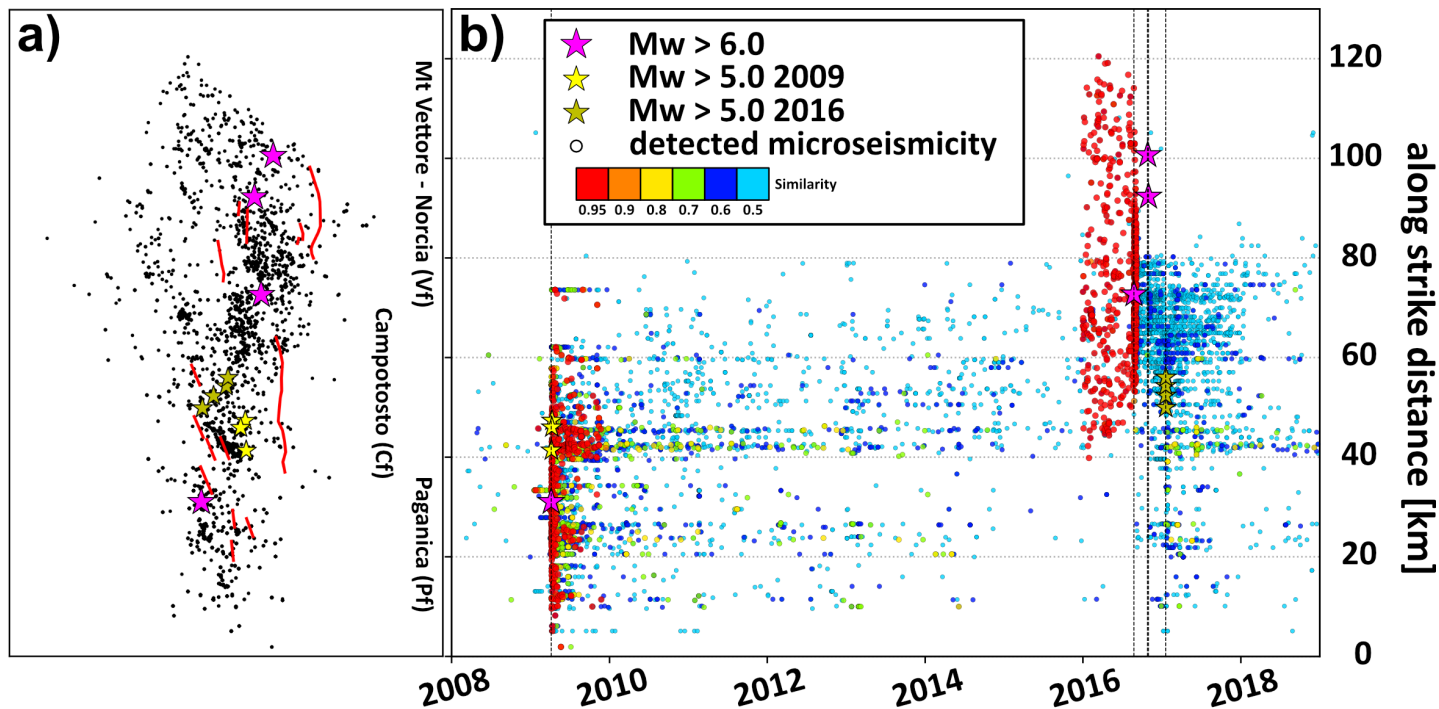
136 We perform a detailed analysis of the available cGPS stations along the Central Apennines from
137 the Alto Tiberina fault system (ATF) to the north and area of L'Aquila 2009 earthquake to the
138 south (Fig 1a). The 2015-2017 time series of the selected stations are analysed following the
139 procedure described in Barzaghi and Borghi (2018) that includes the estimate of discontinuities
140 due to station equipment changes, seismic events, periodic signals and a linear velocity term. The
141 temporal correlations among data have been considered as well. The data were spatially filtered to
142 remove correlated noise using the Principal Component Analysis (PCA), as suggested by Dong et
143 al. (2006) in order to search for transients (Borghi et al., 2016; Gualandi et al., 2016). The residual

144 coordinate time series were analysed using different blind source separation methods (BSS), like
145 Fast Independent Component Analysis (fastICA) and variational Bayesian Independent
146 Component Analysis (vbICA) (Choudrey et al., 2003), as well as PCA. The methodology is
147 described in the Supplementary Material (Appendix-C).
148

149 **3 The 2009 – 2016 sequences**150 **3.1 Detected earthquakes**

151 To evaluate spatial and temporal evolution of earthquake activity within the SZ, we used 1855
 152 templates well distributed along strike and throughout the SZ beneath the causative faults of 2009
 153 (10-12 km depth) and 2016-2017 (8-11 km depth) sequences (Fig 2a). We analyse the continuous
 154 waveform series from 2008 to 2019, and detect 38229 new events in the SZ, ranging between M-
 155 1.5 and M4.7 (Fig S2, S8).

156 Fig 2b shows the along-strike space-time distribution of the newly detected earthquakes (cross-
 157 correlation values above 0.5). For the analysis, the whole SZ volume is divided into three sub-
 158 volumes following the main normal faults: the Paganica fault (Pf), Cf and the Mt. Vettore-Norcia
 159 fault (Vf) (e.g. Basili et al., 2018). Beneath Pf, we detect the foreshocks (Fig S9) to the L’Aquila
 160 mainshock as reported in Sukan et al. (2014). After the L’Aquila mainshock, the detections exhibit
 161 a decay of aftershocks as in Chiaraluce et al. (2011). On the contrary, diffuse earthquakes with
 162 slow decay rate are reported within the SZ under the Cf (Fig 1a, d). We separate the templates of
 163 2016 sequence into foreshocks and early aftershocks (Fig S4a,b) inherent to the August 24th
 164 earthquake covering an 80 km along-strike distance that includes Cf and Vf. For Cf, the detections
 165 reveal a high rate of activity, independent of the templates we use, over the 11-year time span.
 166 Underneath Vf (Fig 1a, c), very few new earthquakes are detected, except in its south-easternmost
 167 part, adjacent to Cf.



168
 169 *Figure 2: a) Locations of selected SZ template earthquakes along strike the Central Italy faults activated in 2009 and 2016*
 170 *sequences. b) Newly detected earthquakes from 2008 until the end of 2018. Colour represents the cross-correlation value of the*
 171 *detection. 2009 sequence undergoes a decay of seismicity along the SZ of Paganica fault while the SZ underneath Campotosto*
 172 *fault shows more constant diffuse earthquake activity. At the beginning of 2016, foreshock activity of 2016 sequence starts along*
 173 *the SZ underneath Campotosto fault and SZ beneath Mt. Vettore fault system.*

174 The cumulative number of events over time and their yearly contributions are reported in Fig S5
 175 and S6. We observe that soon after the 2009 mainshock and its aftershock sequence (September

176 2009), the cumulative number of earthquakes within the SZ beneath Cf overtakes the cumulative
 177 number under the Pf. This is true throughout the years 2010-2015, with few exceptions when a
 178 small sequence starts along Pf (February 2011, February 2012, March 2013). The cumulative
 179 number of earthquakes beneath Cf is steady over the years and characterizes the background
 180 seismicity with small increments over temporal fluctuations (van den Ende et al., 2020).

181 At the end of 2015, the number of detections increased beneath Vf, starting the foreshock sequence
 182 of the August 24th 2016 Mw6 earthquake. Beneath Cf an intensive swarm took place during
 183 February 2016, located adjacent to the future termination of the mainshock slip distribution
 184 (Chiaraluce et al., 2017). After the swarm, the SZ beneath Vf becomes the most active segment.
 185 The diffuse aftershocks that followed the August 24th mainshock are beneath Cf and Vf, where
 186 most of the events took place. After the largest mainshock of October 30th, the activity beneath Cf
 187 increases and by the end of 2016 activity beneath Pf starts to increase. Increased earthquake
 188 production in late December 2016 beneath Cf signals the foreshock sequence of the January 18th
 189 2017 Mw5+ Campotosto earthquakes.

190 We observe (Supplementary material Fig S7) a slow (6 km/year) north-westward migration of
 191 seismicity from the SZ beneath Pf towards the nucleation area of the August 24th 2016 mainshock.
 192 This is followed by a south-eastward migration (0.2 km/day) from the August 24th 2016 nucleation
 193 area towards the hypocentres of Campotosto 2017 earthquakes similar to the observed migration
 194 of seismicity independent of the depth distribution reported by Sebastiani et al. (2019).

195 **3.2 Rupture history for the CF moderate earthquakes**

196 The reported difference between coseismic and aseismic moment released along the Cf during the
 197 2009 and 2017 sequences (e.g. Cheloni et al., 2014; Cheloni et al., 2019) led to the detailed
 198 investigation of the coseismic slip and source geometry of Mw5+ earthquakes on Cf.

199 Seven of the events (except the sub-horizontal June 22nd 2009 M_L 4.4 event along SZ) occurred on
 200 planes with strikes from 142° to 190°, on average 157°, dipping to the southwest (Supplementary
 201 Appendix-A Table A1). Our results confirm the listric geometry of Cf with dip changing over
 202 depth from 50° to 30° (Fig S1).

203 All slip models cover an area of ~18 km per 12 km on the Cf. The patches of maximum slip do
 204 not overlap, and the ruptures evolved mostly up-dip. Similar to the migration observed along the
 205 SZ after 2009 and 2016 sequence, also the 2009 and 2017 Campotosto Mw5+ events follow a
 206 similar pattern and migrate from southeast towards northwest after 2009 and vice-versa after 2016.
 207 Unilateral ruptures are confirmed by directivity in the accelerograms.

208 Source parameters of the 2009 sequence show an average strike of 152° and dip of 48° for the
 209 south-eastern part of the Cf. Scalar seismic moment of $1.73 \cdot 10^{17}$ Nm for the three large
 210 aftershocks and the SZ event of 2009 are close to the value of $1.8 \cdot 10^{17}$ Nm, obtained using point
 211 source inversion method by Scognamiglio et al. (2010). Using SAR and GPS data, Cheloni et al.
 212 (2014) obtained a cumulative scalar seismic moment of $3.17 \cdot 10^{17}$ Nm for co and post-seismic
 213 periods in 2009 and Gualandi et al. (2014) calculated an afterslip of a $2.9 \cdot 10^{17}$ Nm released for
 214 301 days after the 2009 mainshock. This suggests that most of the deformation was aseismic with
 215 half as post-seismic considering negligible sum of the seismic moments released by the rest of
 216 aftershocks (Falcucci et al., 2018).

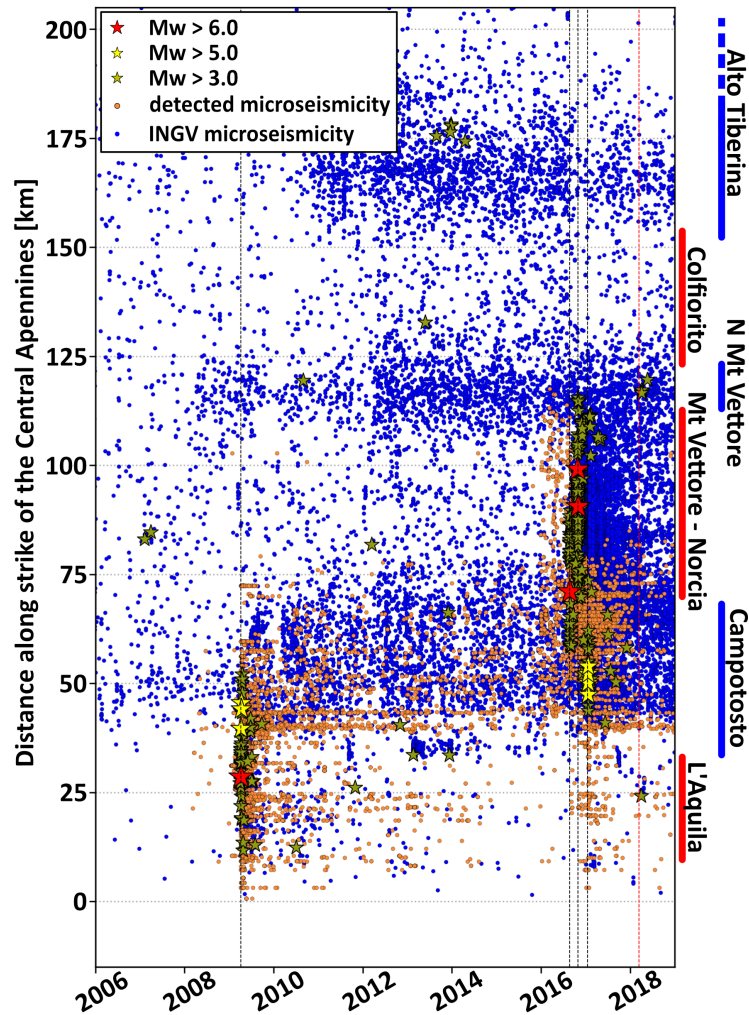
217 Average strike for the 2017 events (north-western part of the Cf) is 161° while average dip is 35°,
 218 13° less than Falcucci et al. (2018) from inversion of surface deformation measured from cGPS
 219 and DInSAR. In their study, the rake angle would play an important role in obtaining the dip angle,
 220 while in our inversions the rake was a well-retrieved parameter. The slip models distribute from

221 depths of 2.5 km to 10 km with a maximum slip of 0.49 m close to Falcucci et al. (2018). We
222 obtain 7.98×10^{17} Nm of scalar seismic energy release during 2017 sequence close to the obtained
223 value by Falcucci et al. (2018). Considering 0.4×10^{17} Nm of scalar seismic moment released by
224 $3.5 < M < 4.9$ aftershocks and the cumulative geodetic moment of 9.29×10^{17} Nm (Cheloni et al.,
225 2019), we reach the same 35% contribution of aseismic strain release suggested by Cheloni et al.
226 (2019).
227 The computed slip history of the $M_w 5+$ events indicate that Cf is partially reactivated along its
228 deeper extent and a rupture up to the surface would require a larger magnitude earthquake as
229 reported by paleoseismologic observations (e.g. Galadini et al., 2003).
230

231 **4 Central Apennines**232 **4.1 Seismicity**

233 We compare our newly constrained catalog with the Italian Seismic Bulletin (Fig 3). We remove
 234 earthquakes shallower than 12 km (removing fixed depth and shallow events) along the Central
 235 Apennines. We observe alternating high and low seismicity rate strands along the strike, showing
 236 similarities to our own findings in the SZ beneath Pf, Cf and Vf. The areas of last moderate
 237 earthquakes in 1997, 2009 and 2016 correspond to strands where seismicity is less diffuse. The
 238 high seismicity rate segments are located in between, namely Campotosto segment, North Mt.
 239 Vettore segment (NVf), and Alto Tiberina segment (Anderlini et al., 2016).

240



241
 242
 243
 244
 245
 246
 247
 248

Figure 3: Seismicity along the strike of Central Apennines. Orange dots represents the new earthquakes obtained in this study while blue dots represent earthquakes deeper than 12 km from INGV earthquake catalog. We observe good spatial correlation between our enhanced catalog in the 2009 and 2016 epicentral areas and INGV catalog. Additionally, similar behaviour is observed along strike of the Central Apennines. Along the segmented SZ we observe segments of high rate seismicity (Campotosto, N. Mt. Vettore, Alto Tiberina – blue vertical lines on the right) and segments with low rate of seismicity (L'Aquila, Mt. Vettore-Norcia, Colfiorito – red vertical lines on the right). Later correspond to the SZ beneath the faults, that ruptured with recent Mw 6+ events.

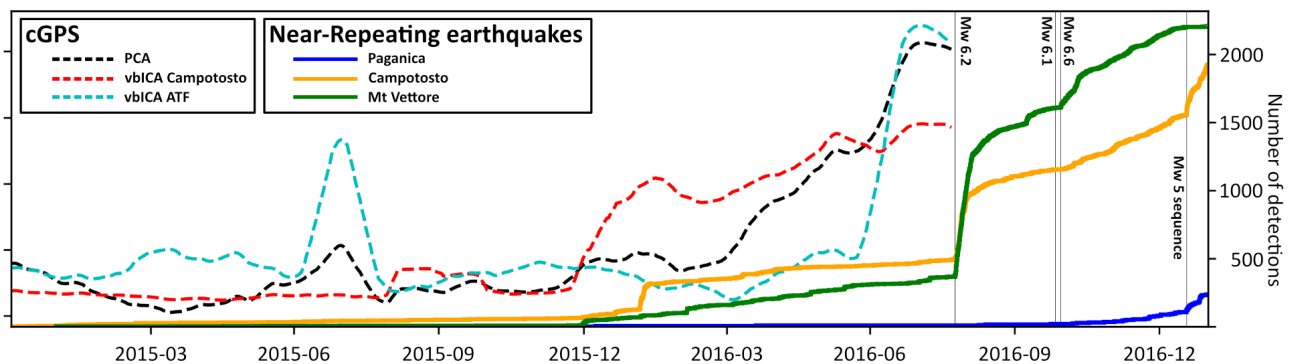
249 4.2. GPS analysis for transient detection

250 The central part of the network (Fig. 1a), where the 2016 M6+ events nucleated represents an
 251 empty zone since no stations were installed in that period or we do not have access to the data.

252 As the analysed period is quite long (from 2012 to the middle of 2018) and is characterized by the
 253 important 2016 seismic sequence, we conducted our analysis dividing the time-series into four
 254 different temporal windows. In this section we focus on the 2015-2016 and 2017-2018 temporal
 255 windows, but all the results of the other periods are reported in Appendix-C.

256 Although the vbICA method has resulted efficient in finding the signal along the Alto Tiberina
 257 fault (ATF) (Gualandi et al., 2017 and Appendix-C), we also applied the PCA method in the
 258 analysis of the period characterized by the 2016 seismic sequence, to find the average behaviour
 259 of the stations and avoid local effects, which allow the vbICA to better identify the signals. We
 260 show the results (Fig. 4) in terms of the second Principal Component (PC2) of the East component.
 261 We observe an increase of values starting at the beginning of 2016 with both northern (ATF) and
 262 southern (Campotosto) GPS station cluster contributing to the PC2. We repeat the analysis splitting
 263 the stations in the ATF and in the Campotosto part. Analysing the two clusters separately allowed
 264 us to point out a similar behaviour of the ATF and Campotosto stations but shifted in time: the
 265 Campotosto stations present this discontinuity in the first vbICA component on January 7th 2016,
 266 with a probability around 94% as detected by the Bayesian test inference (Appendix-C), whereas
 267 the ATF stations present an analogous behaviour seven months later on July 7th with a probability
 268 of 98% (Fig 4).

269 The analysis of the last period, from the end of 2017 to April 2018, involves the cGPS stations set
 270 up after the Mw6.5 October 30th 2016 earthquake. The time-series show (Appendix-C Fig Sc6) the
 271 non-linear effect of the post-seismic deformation. Accordingly we preferred not to fit the data
 272 using any functional models but applied the PCA to describe the deformation. In Appendix-C Fig
 273 Sc7, Sc8 the North and East first principal components are reported. All the stations are affected
 274 by a common signal represented by the linear tectonic rate and the post-seismic deformations,
 275 however a discontinuity is present at the beginning of 2018. Soon after the discontinuity, the
 276 northern extension of the area affected by 3 Mw6+ earthquakes is hit by a series of Mw3.5+
 277 earthquakes with the strongest Mw4.5 on April 10th 2018.
 278



279
 280 *Figure 4: Cumulative number of newly detected earthquakes between 2015 and 2017 and a geodetic transient. Different colours*
 281 *represent different segments of SZ under the shallow normal faults. Dashed black line represents 2nd principal component over*
 282 *all the GPS stations used while red and magenta represent independent components of spatially grouped cGPS stations, around*
 283 *Campotosto and ATF respectively. We observe that deformation is migrating from the south of the system towards north.*

284

285 **5 Conclusions**

286

287 Analysing 11 years of continuous waveforms recorded at multiple seismic stations in Central Italy
288 allowed us to detect more than 38.000 earthquakes within the shear zone (SZ). The detected events
289 and their locations give us insight on the space-time behaviour of the SZ underneath Paganica fault
290 (Pf), Campotosto fault (Cf) and Monte Vettore fault (Vf) before, after and in-between the recent
291 Central Italy earthquake sequences. Pf and Vf are related to the 2009 Mw6.1 L'Aquila earthquake
292 and the 2016 Amatrice-Visso-Norcia Mw6+ earthquakes respectively, which ruptured shallow,
293 SW dipping normal faults. Cf, located in between Pf and Vf, is affected in the aftermath of both
294 2009 and 2016 sequences with earthquakes of Mw5+. We observe different spatial and temporal
295 patterns of earthquakes within the SZ underneath Pf, Cf and Vf.

296 The seismicity rate within the SZ appears to be segmented from south to north along the strike of
297 the fault system (Fig 3). SZ beneath Pf is experiencing an expected decay in its activity after the
298 2009 earthquake reaching a lower rate with very few events after 2014 while the adjacent SZ
299 beneath Cf exhibits a far higher rate in its activity. The SZ beneath Vf shows a very low rate
300 between 2009 up to the end of 2015 when it starts exhibiting a large foreshock sequence, also
301 affecting SZ beneath Cf as well as the above normal faults, prior to the 2016 Mw6+ earthquakes.

302 Our study suggests that Central Apennines are underlain by a sizeable sub-horizontal shear zone
303 that is segmented in its frictional and/or mechanical properties accommodating therefore low and
304 high rates of seismicity at the base of the seismogenic layer. The low rate seismicity segments are
305 beneath high-angle normal faults responsible of the 1997, 2009 and 2016 earthquake sequences.

306 The high rate seismicity segments are beneath listric faults (e.g. Campotosto), and low-angle
307 normal faults like Alto-Tiberina (e.g. Chiaraluce et al., 2014).

308 Analysing 19 cGPS stations show that the start of the 2016 foreshock sequence coincides with a
309 clear geodetic transient that first affected Cf-Pf and later expanded northward affecting ATF. The
310 foreshocks likely correspond to creeping patches accommodating aseismic slow-slip in the
311 preseismic period (e.g. Meng et al., 2014) combined with a gradual unlocking within the plate
312 boundary (e.g. Schurr et al., 2014). The space-time correlations between the seismicity and the
313 geodetic transient and their northward along strike migrations are thus most likely due to an
314 expanding/propagating slow-slip along strike. These results together with the space distribution of
315 the mainshocks show that, most likely, the northward expanding transient was accommodated
316 differently by the reactivated fault system where less-coupled segments alternate with locked
317 segments. Similar behaviour is described in subduction zones (e.g. Rolandone et al., 2018;
318 Radiguet et al., 2016). Furthermore, we argue that the geometry and the frictional properties of the
319 segmented system affects the degree of interseismic coupling. This likely leads to differences in
320 recurrence intervals and maximum magnitude between mature listric faults and younger high-
321 angle normal faults as exhibited by the historical seismicity and paleoseismology across Central
322 Apennines (e.g. Cinti et al., 2018; Falcucci et al., 2018; Galadini et al., 2003, Galli et al., 2019;
323 Guidoboni et al., 2018).

324

325 **Acknowledgments**

326

327 The authors would like to thank Generali group and Generali Italia for the financial support. We
328 would like to thank the Editor and the three reviewers for their useful comments that improved our
329 original manuscript. PyMPA software (Vuan et al., 2018) development is partly supported by the
330 project “Real-time earthquake risk reduction for a reSilient Europe” (RISE), financed by the
331 Horizon 2020 programme of the European Commission. The data are available via the European
332 Integrated Data Archive managed by Istituto Nazionale di Geofisica e Vulcanologia (INGV)
333 (<http://www.orfeus-eu.org/webdc3/>) and Nevada Geodetic Laboratory
334 (<http://geodesy.unr.edu/index.php>).
335

336 **References**

- 337
338 Amato, A., Azzara, R., Chiarabba, C., Cimini, G. B., Cocco, M., Di Bona, M., ... & Basili, A.
339 (1998). The 1997 Umbria-Marche, Italy, earthquake sequence: A first look at the main shocks and
340 aftershocks. *Geophysical Research Letters*, 25(15), 2861-2864,
341 <https://doi.org/10.1029/98GL51842>
342
- 343 Anderlini, L., Serpelloni, E., & Belardinelli, M. E. (2016). Creep and locking of a low-angle
344 normal fault: Insights from the Altotiberina fault in the Northern Apennines (Italy). *Geophysical*
345 *Research Letters*, 43(9), 4321-4329, <https://doi.org/10.1002/2016GL068604>
346
- 347 Aoudia, A., Ismail-Zadeh, A. T., & Romanelli, F. (2007). Buoyancy-driven deformation and
348 contemporary tectonic stress in the lithosphere beneath Central Italy. *Terra Nova*, 19(6), 490-495,
349 <https://doi.org/10.1111/j.1365-3121.2007.00776.x>
350
- 351 Baillard, C., Crawford, W., Ballu, V., Hilbert, C., & Mangeney, A. (2014). Kurtosis- based P and
352 S phase picker designed for local and regional seismic networks, [https://doi.org/](https://doi.org/10.1785/0120120347)
353 [10.1785/0120120347](https://doi.org/10.1785/0120120347)
354
- 355 Barzaghi, R., & Borghi, A. (2018). Theory of second order stationary random processes applied
356 to GPS coordinate time-series. *GPS Solutions*, 22(3), 86, [https://doi.org/10.1007/s10291-018-](https://doi.org/10.1007/s10291-018-0748-4)
357 [0748-4](https://doi.org/10.1007/s10291-018-0748-4)
358
- 359 Basili, R., Burrato, P., Fracassi, U., Kastelic, V., Maesano, F., Tarabusi, G., ... & DISS Working
360 Group. (2018). Database of Individual Seismogenic Sources (DISS), Version 3.2. 1: A compilation
361 of potential sources for earthquakes larger than M 5.5 in Italy and surrounding areas,
362 <https://doi.org/10.6092/INGV.IT-DISS3.2.1>
363
- 364 Borghi, A., Aoudia, A., Javed, F., & Barzaghi, R. (2016). Precursory slow-slip loaded the 2009
365 L'Aquila earthquake sequence. *Geophysical Journal International*, 205(2), 776-784,
366 <https://doi.org/10.1093/gji/ggw046>
367
- 368 Buttinelli, M., Pezzo, G., Valoroso, L., De Gori, P., & Chiarabba, C. (2018). Tectonics inversions,
369 fault segmentation, and triggering mechanisms in the central Apennines normal fault system:
370 Insights from high-resolution velocity models. *Tectonics*, 37(11), 4135-4149,
371 <https://doi.org/10.1029/2018TC005053>
372
- 373 Cheloni, D., Giuliani, R., D'Anastasio, E., Atzori, S., Walters, R. J., Bonci, L., ... & Deninno, F.
374 (2014). Coseismic and post-seismic slip of the 2009 L'Aquila (central Italy) Mw 6.3 earthquake
375 and implications for seismic potential along the Campotosto fault from joint inversion of high-
376 precision levelling, InSAR and GPS data. *Tectonophysics*, 622, 168-185,
377 <https://doi.org/10.1016/j.tecto.2014.03.009>
378
379
380

- 381 Cheloni, D., D'Agostino, N., Scognamiglio, L., Tinti, E., Bignami, C., Avallone, A., ... & Mattone,
 382 M. (2019). Heterogeneous Behavior of the Campotosto Normal Fault (Central Italy) Imaged by
 383 InSAR GPS and Strong-Motion Data: Insights from the 18 January 2017 Events. *Remote*
 384 *Sensing*, 11(12), 1482, <https://doi.org/10.3390/rs11121482>
 385
- 386 Chiarabba, C., De Gori, P., Cattaneo, M., Spallarossa, D., & Segou, M. (2018). Faults geometry
 387 and the role of fluids in the 2016–2017 Central Italy seismic sequence. *Geophysical Research*
 388 *Letters*, 45, 6963–6971. <https://doi.org/10.1029/2018GL077485>
 389
- 390 Chiaraluce, L., Valoroso, L., Piccinini, D., Di Stefano, R., & De Gori, P. (2011). The anatomy of
 391 the 2009 L'Aquila normal fault system (central Italy) imaged by high resolution foreshock and
 392 aftershock locations. *Journal of Geophysical Research: Solid Earth*, 116(B12),
 393 <https://doi.org/10.1029/2011JB008352>
 394
- 395 Chiaraluce, L., Amato, A., Carannante, S., Castelli, V., Cattaneo, M., Cocco, M., ... & Marzorati,
 396 S. (2014). The Alto Tiberina Near Fault Observatory (northern Apennines, Italy). *Annals of*
 397 *Geophysics*, 57(3), <https://doi.org/10.4401/ag-6426>
 398
- 399 Chiaraluce, L., Di Stefano, R., Tinti, E., Scognamiglio, L., Michele, M., Casarotti, E., ... &
 400 Lombardi, A. (2017). The 2016 central Italy seismic sequence: A first look at the mainshocks,
 401 aftershocks, and source models. *Seismological Research Letters*, 88(3), 757-771,
 402 <https://doi.org/10.1785/0220160221>
 403
- 404 Chimera, G., Aoudia, A., Saraò, A., & Panza, G. F. (2003). Active tectonics in Central Italy:
 405 constraints from surface wave tomography and source moment tensor inversion. *Physics of the*
 406 *Earth and Planetary Interiors*, 138(3-4), 241-262, [https://doi.org/10.1016/S0031-9201\(03\)00152-](https://doi.org/10.1016/S0031-9201(03)00152-3)
 407 3
 408
- 409 Choudrey, R. A., & Roberts, S. J. (2003). Variational mixture of Bayesian independent component
 410 analyzers. *Neural computation*, 15(1), 213-252, <https://doi.org/10.1162/089976603321043766>
 411
- 412 Cinti, F. R., Civico, R., Blumetti, A. M., Chiarini, E., La Posta, E., Pantosti, D., ... & Pinzi, S.
 413 (2018). Evidence for surface faulting earthquakes on the Montereale fault system (Abruzzi
 414 Apennines, central Italy). *Tectonics*, 37(9), 2758-2776, <https://doi.org/10.1029/2017TC004780>
 415
- 416 D'Agostino, N., Mantenuto, S., D'Anastasio, E., Giuliani, R., Mattone, M., Calcaterra, S., ... &
 417 Bonci, L. (2011). Evidence for localized active extension in the central Apennines (Italy) from
 418 global positioning system observations. *Geology*, 39(4), 291-294,
 419 <https://doi.org/10.1130/G31796.1>
 420
- 421 Di Carli, S., François-Holden, C., Peyrat, S., & Madariaga, R. (2010). Dynamic inversion of the
 422 2000 Tottori earthquake based on elliptical subfault approximations. *Journal of Geophysical*
 423 *Research: Solid Earth*, 115(B12), <https://doi.org/10.1029/2009JB006358>
 424
 425

- 426 Dong, D., Fang, P., Bock, Y., Webb, F., Prawirodirdjo, L., Kedar, S., & Jamason, P. (2006).
 427 Spatiotemporal filtering using principal component analysis and Karhunen-Loeve expansion
 428 approaches for regional GPS network analysis. *Journal of geophysical research: solid*
 429 *earth*, 111(B3), <https://doi.org/10.1029/2005JB003806>.
 430
- 431 Falcucci, E., Gori, S., Bignami, C., Pietrantonio, G., Melini, D., Moro, M., ... & Galadini, F.
 432 (2018). The Campotosto seismic gap in between the 2009 and 2016–2017 seismic sequences of
 433 central Italy and the role of inherited lithospheric faults in regional seismotectonic
 434 settings. *Tectonics*, 37(8), 2425-2445, <https://doi.org/10.1029/2017TC004844>
 435
- 436 Galadini, F., & Galli, P. (2003). Paleoseismology of silent faults in the Central Apennines (Italy):
 437 the Mt. Vettore and Laga Mts. faults. *Annals of Geophysics*, <https://doi.org/10.4401/ag-3457>
 438
- 439 Galli, P., Galderisi, A., Peronace, E., Giaccio, B., Hajdas, I., Messina, P., ... & Polpetta, F. (2019).
 440 The awakening of the dormant Mount Vettore fault (2016 central Italy earthquake, Mw 6.6):
 441 paleoseismic clues on its millennial silences. *Tectonics*, 38(2), 687-705,
 442 <https://doi.org/10.1029/2018TC005326>
 443
- 444 Gibbons, S. J., & Ringdal, F. (2006). The detection of low magnitude seismic events using array-
 445 based waveform correlation. *Geophysical Journal International*, 165(1), 149-166,
 446 <https://doi.org/10.1111/j.1365-246X.2006.02865.x>
 447
- 448 Gualandi, A., Serpelloni, E., & Belardinelli, M. E. (2014). Space–time evolution of crustal
 449 deformation related to the M w 6.3, 2009 L'Aquila earthquake (central Italy) from principal
 450 component analysis inversion of GPS position time-series. *Geophysical Journal*
 451 *International*, 197(1), 174-191, <https://doi.org/10.1093/gji/ggt522>
 452
- 453 Gualandi, A., Serpelloni, E., & Belardinelli, M. E. (2016). Blind source separation problem in GPS
 454 time series. *Journal of Geodesy*, 90(4), 323-341, <https://doi.org/10.1007/s00190-015-0875-4>
 455
- 456 Gualandi, A., Nichele, C., Serpelloni, E., Chiaraluce, L., Anderlini, L., Latorre, D., ... & Avouac,
 457 J. P. (2017). Aseismic deformation associated with an earthquake swarm in the northern Apennines
 458 (Italy). *Geophysical Research Letters*, 44(15), 7706-7714,
 459 <https://doi.org/10.1002/2017GL073687>
 460
- 461 Guidoboni, E., Ferrari, G., Mariotti, D., Comastri, A., Tarabusi, G., Sgattoni, G., & Valensise, G.
 462 (2018). CFTI5Med, Catalogo dei Forti Terremoti in Italia (461 aC-1997) e nell'area Mediterranea
 463 (760 aC-1500), <https://doi.org/10.6092/ingv.it-cfti5>
 464
- 465 Herrmann, R. B., Malagnini, L., & Munafò, I. (2011). Regional Moment Tensors of the 2009
 466 L'Aquila Earthquake Sequence Regional Moment Tensors of the 2009 L'Aquila Earthquake
 467 Sequence. *Bulletin of the Seismological Society of America*, 101(3), 975-993,
 468 <https://doi.org/10.1785/0120100184>
 469
 470
 471

- 472 Improta, L., Latorre, D., Margheriti, L., Nardi, A., Marchetti, A., Lombardi, A. M., ... & Moretti,
 473 M. (2019). Multi-segment rupture of the 2016 Amatrice-Visso-Norcia seismic sequence (central
 474 Italy) constrained by the first high-quality catalog of Early Aftershocks. *Scientific reports*, 9(1), 1-
 475 13, <https://doi.org/10.1038/s41598-019-43393-2>
 476
- 477 Krischer, L., Megies, T., Barsch, R., Beyreuther, M., Lecocq, T., Caudron, C., & Wassermann, J.
 478 (2015). ObsPy: A bridge for seismology into the scientific Python ecosystem. *Computational*
 479 *Science & Discovery*, 8(1), 014003, <https://doi.org/10.1088/1749-4699/8/1/014003>
 480
- 481 Meng, L., Huang, H., Bürgmann, R., Ampuero, J. P., & Strader, A. (2015). Dual megathrust slip
 482 behaviors of the 2014 Iquique earthquake sequence. *Earth and Planetary Science Letters*, 411,
 483 177-187, <https://doi.org/10.1016/j.epsl.2014.11.041>
 484
- 485 Momeni, S. M., Aoudia, A., Tatar, M., Twardzik, C., & Madariaga, R. (2019). Kinematics of the
 486 2012 Ahar–Varzaghan complex earthquake doublet (M w6. 5 and M w6. 3). *Geophysical Journal*
 487 *International*, 217(3), 2097-2124, <https://doi.org/10.1093/gji/ggz100>
 488
- 489 Peng, Z., & Zhao, P. (2009). Migration of early aftershocks following the 2004 Parkfield
 490 earthquake. *Nature Geoscience*, 2(12), 877-881, <https://doi.org/10.1038/ngeo697>
 491
- 492 Porreca, M., Minelli, G., Ercoli, M., Brobia, A., Mancinelli, P., Cruciani, F., ... & Cannata, A.
 493 (2018). Seismic reflection profiles and subsurface geology of the area interested by the 2016–2017
 494 earthquake sequence (Central Italy). *Tectonics*, 37(4), 1116-1137,
 495 <https://doi.org/10.1002/2017TC004915>
 496
- 497 Radiguet, M., Perfettini, H., Cotte, N., Gualandi, A., Valette, B., Kostoglodov, V., ... & Campillo,
 498 M. (2016). Triggering of the 2014 M w 7.3 Papanao earthquake by a slow slip event in Guerrero,
 499 Mexico. *Nature Geoscience*, 9(11), 829-833, <https://doi.org/10.1038/ngeo2817>
 500
- 501 Rolandone, F., Nocquet, J. M., Mothes, P. A., Jarrin, P., Vallée, M., Cubas, N., ... & Font, Y.
 502 (2018). Areas prone to slow slip events impede earthquake rupture propagation and promote
 503 afterslip. *Science advances*, 4(1), eaao6596, <https://doi.org/10.1126/sciadv.aao6596>
 504
- 505 Ross, Z. E., Trugman, D. T., Hauksson, E., & Shearer, P. M. (2019). Searching for hidden
 506 earthquakes in Southern California. *Science*, 364(6442), 767-771,
 507 <https://doi.org/10.1126/science.aaw6888>
 508
- 509 Rovida, A., Camassi, R., Gasperini, P., & Stucchi, M. (2011). Catalogo parametrico dei terremoti
 510 italiani, <https://doi.org/10.13127/CPTI/CPTI15.2>
 511
- 512 Ruiz, S., & Madariaga, R. (2013). Kinematic and dynamic inversion of the 2008 Northern Iwate
 513 earthquake. *Bulletin of the Seismological Society of America*, 103(2A), 694-708,
 514 <https://doi.org/10.1785/0120120056>
 515
 516

- 517 Schurr, B., Asch, G., Hainzl, S., Bedford, J., Hoechner, A., Palo, M., ... & Oncken, O. (2014).
 518 Gradual unlocking of plate boundary controlled initiation of the 2014 Iquique earthquake. *Nature*,
 519 512(7514), 299-302, <https://doi.org/10.1038/nature13681>
 520
- 521 Scognamiglio, L., Tinti, E., Michelini, A., Dreger, D. S., Cirella, A., Cocco, M., ... & Piatanesi, A.
 522 (2010). Fast determination of moment tensors and rupture history: What has been learned from the
 523 6 April 2009 L'Aquila earthquake sequence. *Seismological Research Letters*, 81(6), 892-906,
 524 <https://doi.org/10.1785/gssrl.81.6.892>
 525
- 526 Sebastiani, G., Govoni, A., & Pizzino, L. (2019). Aftershock Patterns in Recent Central Apennines
 527 Sequences. *Journal of Geophysical Research: Solid Earth*, 124(4), 3881-3897,
 528 <https://doi.org/10.1029/2018JB017144>
 529
- 530 Shelly, D. R., Beroza, G. C., & Ide, S. (2007). Non-volcanic tremor and low-frequency earthquake
 531 swarms. *Nature*, 446(7133), 305-307, <https://doi.org/10.1038/nature05666>
 532
- 533 Soldati, G., Zaccarelli, L., Faenza, L., & Michelini, A. (2015). Monitoring of crustal seismic
 534 velocity variations in the L'Aquila fault zone inferred from noise cross-correlation. *Geophysical*
 535 *Journal International*, 202(1), 604-611, <https://doi.org/10.1093/gji/ggv172>
 536
- 537 Sugan, M., Kato, A., Miyake, H., Nakagawa, S., & Vuan, A. (2014). The preparatory phase of the
 538 2009 Mw 6.3 L'Aquila earthquake by improving the detection capability of low-magnitude
 539 foreshocks. *Geophysical Research Letters*, 41(17), 6137-6144,
 540 <https://doi.org/10.1002/2014GL061199>
 541
- 542 Twardzik, C., Madariaga, R., Das, S., & Custódio, S. (2012). Robust features of the source process
 543 for the 2004 Parkfield, California, earthquake from strong-motion seismograms. *Geophysical*
 544 *Journal International*, 191(3), 1245-1254, <https://doi.org/10.1111/j.1365-246X.2012.05653.x>
 545
- 546 Valoroso, L., Chiaraluce, L., Piccinini, D., Di Stefano, R., Schaff, D., & Waldhauser, F. (2013).
 547 Radiography of a normal fault system by 64,000 high-precision earthquake locations: The 2009
 548 L'Aquila (central Italy) case study. *Journal of Geophysical Research: Solid Earth*, 118(3), 1156-
 549 1176, <https://doi.org/10.1002/jgrb.50130>
 550
- 551 van den Ende, M. P., & Ampuero, J. P. (2020). On the statistical significance of foreshock
 552 sequences in Southern California. *Geophysical Research Letters*, 47(3), e2019GL086224.
 553
- 554 Vičić, B., Aoudia, A., Javed, F., Foroutan, M., & Costa, G. (2019). Geometry and mechanics of
 555 the active fault system in western Slovenia. *Geophysical Journal International*, 217(3), 1755-
 556 1766, <https://doi.org/10.1093/gji/ggz118>
 557
- 558 Vuan, A., Sugan, M., Chiaraluce, L., & Di Stefano, R. (2017). Loading rate variations along a
 559 midcrustal shear zone preceding the Mw6. 0 earthquake of 24 August 2016 in Central Italy.
 560 *Geophysical Research Letters*, 44(24), <https://doi.org/10.1002/2017GL076223>
 561

- 562 Vuan, A., Sukan, M., Amati, G., & Kato, A. (2018). Improving the Detection of Low-Magnitude
563 Seismicity Preceding the M w 6.3 L'Aquila Earthquake: Development of a Scalable Code Based
564 on the Cross Correlation of Template Earthquakes. *Bulletin of the Seismological Society of*
565 *America*, 108(1), 471-480, <https://doi.org/10.1785/0120170106>
566
- 567 Walters, R. J., Gregory, L. C., Wedmore, L. N. J., Craig, T. J., McCaffrey, K., Wilkinson, M., ...
568 & Iezzi, F. (2018). Dual control of fault intersections on stop-start rupture in the 2016 Central Italy
569 seismic sequence. *Earth and Planetary Science Letters*, 500, 1-14,
570 <https://doi.org/10.1016/j.epsl.2018.07.043>
571

572 **References From the Supporting Information**

- 573
- 574 Blewitt, G., Hammond, W. C., & Kreemer, C. (2018). Harnessing the GPS data explosion for
575 interdisciplinary science. *Eos*, 99, 1-2, <https://doi.org/10.1029/2018EO104623>.
- 576
- 577 Borghi A., Aoudia A., Riva R., Barzaghi R. (2009). GPS monitoring and earthquake prediction: a
578 success story towards a useful integration. *Tectonophysics*, 465, pp 177-189, ISSN 0040-1951,
579 doi: 10.1016/j.tecto.2008.11.022
- 580
- 581 Borghi, A., Cannizzaro, L., & Vitti, A. (2012). Advanced techniques for discontinuity detection in
582 GNSS coordinate time-series. An Italian case study. In *Geodesy for Planet Earth*(pp. 627-634).
583 Springer, Berlin, Heidelberg , https://doi.org/10.1007/978-3-642-20338-1_77
- 584
- 585 Choudrey. R.A., Variational Methods for Bayesian Independent Component Analysis. Pattern
586 analysis and machine learning - robotics research group, University of Oxford, 2002.
- 587
- 588 Cotton, F., & Coutant, O. (1997). Dynamic stress variations due to shear faults in a plane-layered
589 medium. *Geophysical Journal International*, 128(3), 676-688, <https://doi.org/10.1111/j.1365-246X.1997.tb05328.x>
- 590
- 591
- 592 Hyvärinen, A., & Oja, E. (2000). Independent component analysis: algorithms and
593 applications. *Neural networks*, 13(4-5), 411-430, [https://doi.org/10.1016/S0893-6080\(00\)00026-5](https://doi.org/10.1016/S0893-6080(00)00026-5)
- 594
- 595 Sambridge, M. (1999). Geophysical inversion with a neighbourhood algorithm—I. Searching a
596 parameter space. *Geophysical journal international*, 138(2), 479-494,
597 <https://doi.org/10.1046/j.1365-246X.1999.00876.x>
- 598
- 599 Sambridge, M. (1999). Geophysical inversion with a neighbourhood algorithm—II. Appraising
600 the ensemble. *Geophysical Journal International*, 138(3), 727-746,
601 <https://doi.org/10.1046/j.1365-246x.1999.00900.x>
- 602
- 603 Schmedes, J., Archuleta, R. J., & Lavallée, D. (2010). Correlation of earthquake source parameters
604 inferred from dynamic rupture simulations. *Journal of Geophysical Research: Solid*
605 *Earth*, 115(B3), <https://doi.org/10.1029/2009JB006689>
- 606
- 607 Silverii, Francesca, et al. "Transient crustal deformation from karst aquifers hydrology in the
608 Apennines (Italy)." *Earth and Planetary Science Letters* 506 (2019): 23-37,
609 <https://doi.org/10.1016/j.epsl.2018.10.019>
- 610
- 611 Spudich, P., & Miller, D. P. (1990). Seismic site effects and the spatial interpolation of earthquake
612 seismograms: results using aftershocks of the 1986 North Palm Springs, California,
613 earthquake. *Bulletin of the Seismological Society of America*, 80(6A), 1504-1532.
- 614
- 615 Wdowinski, S., Bock, Y., Zhang, J., Fang, P., & Genrich, J. (1997). Southern California
616 permanent GPS geodetic array: Spatial filtering of daily positions for estimating coseismic and

617 postseismic displacements induced by the 1992 Landers earthquake. *Journal of Geophysical*
618 *Research: Solid Earth*, 102(B8), 18057-18070, <https://doi.org/10.1029/97JB01378>